Int. J. Ind. Chem. 2026; 17(1): 41-50

International Journal of Industrial Chemistry (IJIC)

https://doi.org/10.57647/ijic.2026.1701.05

Research Article

Synthesis and Application of a Third-Generation Magnetic Graphene Oxide Nanoadsorbent for High-Efficiency Aflatoxin Removal

Zahra Shafiee[1], Fariba Tadayon[1,*], Rouhollah Karimi-Osboo[2], Homayon Ahmad Panahi[3], Elham Moniri[4]

[1] *Department of Chemistry, NT.C., Islamic Azad University, Tehran, Iran*

[2] *Mycotoxins Research Laboratory, Agricultural Research Education and Extension Organization (AREEO), Iranian Research Institute of Plant Protection, Shiraz, Iran*

[3] *Department of Chemistry, CT.C., Islamic Azad University, Tehran, Iran*

[4] *Department of Chemistry, VaP.C., Islamic Azad University, Varamin, Iran*

[*] **Corresponding authors:** fariba.tadayon@iau.ac.ir

Article History:

Received:
19 January 2026

Revised:
03 February 2026

Accepted:
18 March 2026

Published in Issue:
31 March 2026

Abstract

A novel graphene oxide (GO)-based nanocomposite was developed for efficient adsorption and extraction of aflatoxins from contaminated solutions. Synthesis began with the activation of cyanuric chloride, followed by extension with the ligand para-aminobenzoic acid over three generations.To enhance adsorption efficiency and facilitate separation, the final adsorbent was coated with magnetic nanoparticles (Fe_3O_4), yielding a magnetic nanocomposite. The structure and physicochemical properties of the nanocomposite were characterized using FTIR, TGA, XRD, FE-SEM, EDX, and VSM. The adsorbent's performance in aflatoxin extraction was evaluated by HPLC, which showed high adsorption capacity and recovery efficiency. The adsorption isotherm data fit the Langmuir model well (R^2 = 0.9977), indicating uniform monolayer adsorption. A pseudo-second-order model (R^2 = 0.9958) further confirmed that the experimental data were consistent with the adsorption kinetics.The synthesized nanoadsorbent demonstrated exceptional efficiency in removing aflatoxins from contaminated samples, underscoring its potential as an effective material for sample pretreatment and separation in food and environmental contexts.

Keywords: Aflatoxin adsorption; Dendrimer; Graphene oxide; Magnetic nanocomposite; Nanoadsorbent

Cite this article: Shafiee Z, Tadayon F, Karami-Osboo R, Ahmad Panahi H, Moniri E. Altitude Dependent Flavonoid Glycoside Profiles of Iranian *Morus nigra* L. Leaves Analyzed by UPLC-DAD-QTOF/MS. Int. J. Ind. Chem. 2026; 17(1): 41-50. https://doi.org/10.57647/ijic.2026.1701.05

1. Introduction

Aflatoxins (AFs) are toxic, low-molecular-weight secondary metabolites produced by specific fungal species. These compounds contaminate roughly a quarter of the world's agricultural produce, posing a significant threat to global food safety and quality [1]. AFs are classified as mutagenic, teratogenic, carcinogenic, and immunosuppressive [2, 3]. To date, over 300 mycotoxins have been reported as toxic secondary metabolites produced by fungi in various food and feed products. Among these, aflatoxins, primarily produced by *Aspergillus* species, pose the most serious global threat because of their high toxicity and widespread distribution. The primary forms of aflatoxins are classified into four major types (B1, B2, G1, and G2) and two key

hydroxylated metabolites (M1 and M2). Among these, AFB1 is recognized as the most prevalent and potent. Milk samples often contain the hydroxylated metabolites AFM1 and AFM2 [5-7. The European Union has imposed stringent limits of 2 µg kg^{-1} for AFB1 and 4 µg kg^{-1} for total aflatoxins on a range of agricultural products, including peanuts, tree nuts, dried fruits, and cereals, since 1998 [3]. As per EU Regulation 2023/915, the allowable limits for aflatoxins are 2 µg kg^{-1} for AFB1 and 4 µg kg^{-1} for total aflatoxins. Due to its heightened toxicity, a much stricter maximum of 0.1 µg kg^{-1} for AFB1 is enforced for infant and young children's food [8-10].

Accurate determination of toxic compounds in food is vital for monitoring food quality and preventing exposure to harmful substances. Several sample preparation techniques, including DLLME, QuEChERS, SPE, and MDSPE, have been developed to enhance sensitivity and minimize matrix effects before analysis. Among them, magnetic adsorbents have attracted significant attention due to their simple separation process, which eliminates centrifugation and filtration steps by employing an external magnet.

Liquid chromatography techniques, including HPLC and LC-MS, as well as fluorescence and colorimetric detection, are the most common methods for quantitative mycotoxin analysis. Although chromatographic methods offer high sensitivity and selectivity, they have several limitations, such as labor-intensive sample preparation, high cost, and low antibody stability [12].

Furthermore, access to HPLC analysis is often limited. Therefore, the present study focused on designing an efficient and economical adsorbent capable of selectively extracting aflatoxins from food samples. Dendrimers are a unique class of highly branched macromolecules, with successive branching from a central nucleus yielding a well-organized core–shell architecture [13].

Owing to their distinct structure and physicochemical properties, dendrimers have attracted increasing attention in diverse fields. Their features include highly branched, monodisperse structures, spherical morphology, and tunable surface functionalities. Amphiphilic dendrimers are reported to display micelle-like behavior [14], while JDs act as synthetic surfactants by combining hydrophilic and hydrophobic dendritic domains within a single macromolecule [13].

Given the molecular structure of aflatoxins, dendrimers can serve as effective adsorbents for their separation, preconcentration, and determination. Graphene has garnered considerable interest due to its low toxicity, distinctive structure, high biomolecular loading capacity, straightforward synthesis, and cost-effectiveness [15, 16].

In recent years, nanotechnology has rapidly advanced across various scientific fields. Nanoparticles, owing to their small size (<100 nm), high dispersion, reactivity, and large surface area, demonstrate outstanding adsorption capabilities [17, 18].

The magnetic properties of MNPs can be significantly enhanced by varying their compositions. MNPs typically include iron-based, metallic, and alloy nanoparticles [19]. Because of their extensive applications in medicine, biotechnology, materials science, and environmental research, the synthesis of MNPs has attracted significant attention.

In this study, a graphene oxide–dendrimer-based nanocomposite (3D/GO/CNC@PAHA-AN) was designed and synthesized for the removal of aflatoxin. The dendrimer was extended to three generations. Following structural characterization, the synthesized nanocomposite was used to extract aflatoxin, and the extraction conditions were optimized.

2. Methodology

2.1. Chemicals

Graphene oxide, iron (II) chloride tetrahydrate, iron (III) chloride hexahydrate, cyanuric chloride, 1,3-phenylenediamine, 1,4-dioxane, xylene, methanol, acrylonitrile, TEA, Raney R-Ni, hydrazinium monohydrate, and PAHA as a dendrimer ligand. Aflatoxin standards (1000 mg L^{-1}) were obtained from Sigma-Aldrich. All solutions were prepared with ultrapure deionized water.

2.2. Instruments

The morphology and structural characteristics of the nanomaterial were investigated using FE-SEM (TESCAN MIRA3, Czech Republic). FTIR spectroscopy (Thermo Avatar) was used to identify functional groups on the adsorbent. Spectra were collected at room temperature using the KBr pellet technique under dry air.

The crystalline phase and structural properties of the material were analyzed using XRD (Philips PW1730, Netherlands) with Cu Kα radiation (λ = 1.540598 Å, 40 kV, 30 mA). Magnetic properties were measured using a VSM (MDKB) under a vertical magnetic field of 0-1 T. Thermal stability and degradation behavior were assessed by TGA (Q600). Elemental composition was determined using EDX in conjunction with SEM. The analysis was carried out on a Waters Breeze chromatography platform. The instrument configuration included a Kobra cell for post-column derivatization and a multi-wavelength detection system. A Waters Nova-Pak® C-18 reversed-phase column (3.9 × 150 mm, 4 µm) was used for separation at 35 °C. An isocratic elution was employed with a mobile phase of acidified water, methanol, and acetonitrile (6:4:1, v/v/v). This mixture was supplemented with 120 mg L^{-1} of KBr and 350 mL of 4 M HNO_3. System

operation, data collection, and analysis were managed by Breeze software [2].

2.3. Creation of the standard solution

The AFs Standards were purchased from Sigma-Aldrich (St. Louis, MO, USA). Following AOAC guidelines, the absorbance of each standard was measured at 365 nm using a PerkinElmer UV spectrophotometer after preparing 1000 ng mL^{-1} solutions in HPLC-grade methanol. A combined stock solution was prepared in methanol, containing AFB_1 and AFG_1 at 1000 ng mL^{-1} and AFB_2 and AFG_2 at 200 ng mL^{-1}, and stored in amber vials at −20 °C. This stock solution was used for recovery experiments and was diluted in series to prepare working standard mixtures for HPLC calibration curves [20].

2.4. Synthesis of the nano adsorbent

2.4.1. *Synthesis of amphiphilic dendrimer (GO/CNC@PAHA-AN) on graphene oxide substrate*

Graphene oxide (0.5 g), prepared by the modified Hummers' procedure [21], was dispersed in 25 mL of cyanuric chloride solution in a 50 mL round-bottom flask. The suspension was stirred magnetically at room temperature for 10 h. After filtration, the precipitate was washed thoroughly with distilled water until neutral, then immersed in petroleum ether for 24 h to remove any physically adsorbed cyanuric chloride. The solid was filtered and dried at room temperature. Following this, 0.2 g of PAHA was dissolved in 2 mL of 1,4-dioxane and added to the solid.

The mixture was refluxed at 90 °C for 9 h. The modified GO was dispersed in 20 mL of anhydrous methanol, treated with acrylonitrile (3 g) and TEA (2.3 g), and stirred under nitrogen at 80 °C for 1 h. The product was washed thoroughly with methanol to yield the first-generation (G1) dendrimer. Nitro groups were converted to primary amines by catalytic hydrogen transfer using Raney Nickel (0.1 g) and hydrazine monohydrate (2 mL) under an inert nitrogen atmosphere at room temperature for 4 h.

The product was washed with methanol to obtain the reduced G1 dendrimer. Higher-generation dendrimers (G2, G3) were synthesized by repeating the steps involving cyanuric chloride, PAHA, acrylonitrile, and subsequent nitro group reduction.

2.4.2. *Synthesis of magnetic nanoparticles (Fe_3O_4 NPs)*

$FeCl_2{\cdot}4H_2O$ (6.70 g) and FeCl2·4H2O (2 g) were mixed in 230 mL of distilled water and agitated vigorously at 25 °C for 30 minutes. The solution was deoxygenated with nitrogen at 80 °C for 30 min. Then, a 25% ammonia solution was added dropwise until a black precipitate formed, indicating the formation of Fe_3O_4 nanoparticles. The nitrogen atmosphere was restored, and the mixture was stirred at 25 °C for 2 h, then ultrasonicated for 7 min. The precipitate was collected with a magnet; the resulting material was washed several times with deionized water and ethanol, then dried at 70 °C in an oven [21].

2.4.3. *Fabrication of 3D/GO/CNC@PAHA-AN via Fe_3O_4 incorporation*

GO/CNC@PAHA-AN (0.1 g) was uniformly dispersed in 50 mL of distilled water, and the pH was adjusted to 11 by slowly adding 25% ammonia solution. Fe_3O_4 (0.965 g) was then added, and the mixture was ultrasonicated for 5 min. After synthesis, the mixture was heated at 90 °C for 6 hours without stirring. The final product was magnetically separated, washed with deionized water and ethanol, frozen overnight at –25 °C, and lyophilized at –70 °C for 24 hours [22].

2.5. Evaluation of adsorption capacity

To assess adsorption capacity, 50 mg of the synthesized nanoadsorbent was placed in a Falcon tube containing 1 mL of a methanol–water mixture (60:40, v/v). A blank control without any adsorbent was also prepared. Each tube received 10 µL of a 1000 ng g^{-1} aflatoxin standard solution, was vortexed for 1 minute, and then centrifuged at 2000 rpm for 3 minutes. The supernatant was collected and analyzed by HPLC. The adsorption capacity (Q) was calculated using the following equation:

$$Q = Co - C_f / m \times V \quad (1)$$

In this equation, Q represents the equilibrium adsorption capacity (mg g^{-1}), C_0 and C_f are the initial and equilibrium concentrations of aflatoxin (mg L^{-1}), V is the volume of the solution (mL), and m indicates the mass of the adsorbent (g).

3. Result and discussion

3.1. Stepwise synthesis of graphene oxide–based dendrimer

Graphene oxide (GO) was selected as the central platform for the construction of dendrimers. The stepwise synthetic pathway is schematically illustrated in Fig. 1. To activate the GO surface, cyanuric chloride ($C_3N_3Cl_3$) was employed. This compound contains a triazine ring with three reactive chlorine atoms, which undergo nucleophilic substitution by hydroxyl (–OH) and carboxyl (–COOH) groups in the GO framework. In the subsequent step, the remaining chlorine atoms on the triazine ring reacted with the amino groups of PAHA.

10.57647/ijic.2026.1701.05

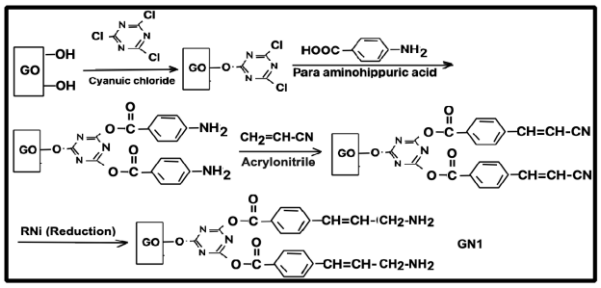

Figure 1. Schematic representation of the synthesis of the first-generation 3D/GO/CNC@PAHA-AN dendrimer

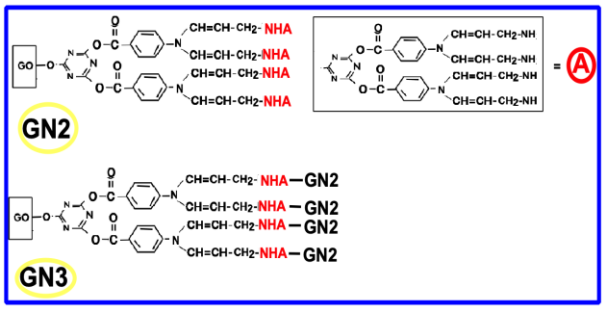

Figure 2. Schematic representation of the synthesis of second- and third-generation 3D/GO/CNC@PAHA-AN dendrimers

This nucleophilic substitution formed amide bonds, generating the primary branches of the dendrimer on the GO surface, corresponding to the first G1. To expand the branching, acrylonitrile (CH_2=CH–CN) was introduced. The free amine groups from the previous step reacted with acrylonitrile via Michael addition, introducing terminal nitrile groups. These terminal nitriles were then reduced to primary amines under reductive conditions using Raney Nickel (R-Ni) as a catalyst [23]. This reduction step not only stabilized the terminal groups but also revitalized the active amino sites required to promote the synthesis of higher generations of the dendrimer. The sequence of surface activation with cyanuric chloride, PAHA grafting, acrylonitrile addition, and nitrile reduction with Raney Nickel was repeated to synthesize second- (G2) and third-generation (G3) dendrimers, as depicted in Fig. 2. At each successive generation, the surface density of amino groups increased, enhancing the capacity to interact with metal ions, organic molecules, biomolecules, and toxins such as aflatoxins. This stepwise synthetic strategy enabled precise control over the dendrimer's architecture, making it a novel multifunctional nanoplatform with significant potential in nanotechnology, biomedicine, and environmental purification.

3.2. Characterization

3.2.1. *FT-IR spectroscopy*

FT-IR spectra were recorded to monitor and confirm the stepwise synthesis of the dendrimer on the graphene oxide (GO) surface. The spectra for the first (c), second (b), and third (a) generations of the magnetic nanostructure 3D/GO/CNC@PAHA-AN are presented in Fig. 3.

In the first-generation spectrum (c), a broad absorption band at approximately 3447 cm^{-1} is attributed to O–H or N–H stretching vibrations, indicating hydroxyl or amine functionalities. A distinct peak at 1577 cm^{-1} corresponds to C=N stretching in the triazine ring (derived from cyanuric chloride), confirming successful grafting of the first dendrimer layer onto the GO surface. Additional peaks at 1414 cm^{-1} and 1078 cm^{-1} are assigned to C–N and C–O stretching, respectively. The fingerprint region shows characteristic peaks at 872, 782, and 649 cm^{-1}, further confirming the presence of aromatic and triazine ring structures.

In the second-generation spectrum (b), the intensity of the O–H and N–H bands near 3463 cm^{-1} increases, and a new peak at 2924 cm^{-1} appears, corresponding to aliphatic C–H stretching and attributed to the introduction of the organic ligand PAHA. The persistence of the 1577 cm^{-1} peak indicates the stability of the triazine structure in the second layer. The significant enhancement of peaks between 1414 and 1021 cm^{-1} is associated with increased C–N and C–O bonding due to dendrimer branch growth. Furthermore, the fingerprint region shows stronger, more defined peaks than in the first generation, reflecting a more complex molecular structure. In the third-generation spectrum (a), the most intense and broad absorption band is observed at 3458 cm^{-1}, indicating a substantial increase in amine groups within the dendrimer structure. Peaks at 1580 and 1576 cm^{-1} confirm the continued presence of C=N bonds in the triazine ring.

Peaks at 1413 cm^{-1} and 1090 cm^{-1} appear with greater intensity than in the previous generations, supporting the formation of additional C–N and C–O bonds due to dendrimer branching. The fingerprint region exhibits distinct, well-resolved peaks, indicating increased structural complexity and three-dimensional growth of the third-generation dendrimer [24, 25]. Overall, FT-IR analysis confirms the successful stepwise synthesis of the dendrimer on the GO surface. The gradual increase in the intensity and diversity of peaks corresponding to the C=N, N–H, and C–N functional groups from the first to the third generation provides strong evidence for the progressive enhancement of organic-moiety density and the expansion of the dendritic architecture during synthesis.

3.2.2. *VSM analysis of samples*

The magnetic properties of the 3D/GO/CNC@PAHA-AN nanocomposite were evaluated using a VSM under a magnetic field of ±10,000 Oe. As shown in Fig. 4, the magnetization (emu g^{-1}) was plotted as a function of the applied magnetic field, and the curve exhibits the characteristic S-shaped behavior of ferromagnetic materials.

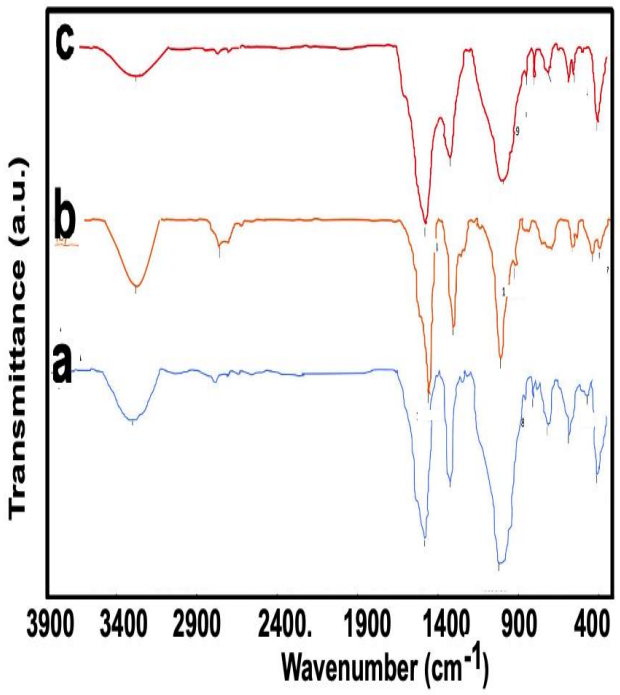

Figure 3. FT-IR spectra of the synthesized graphene oxide-based dendrimers: first generation (c, GN1), second generation (b, GN2), and third generation (a, GN3)

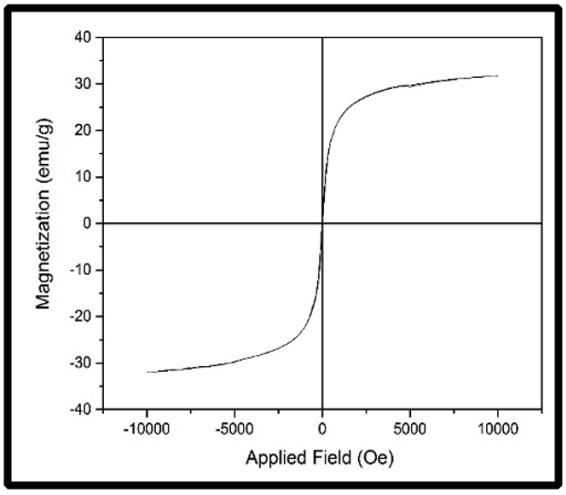

Figure 4. VSM curve of the 3D/GO/CNC@PAHA-AN dendrimer

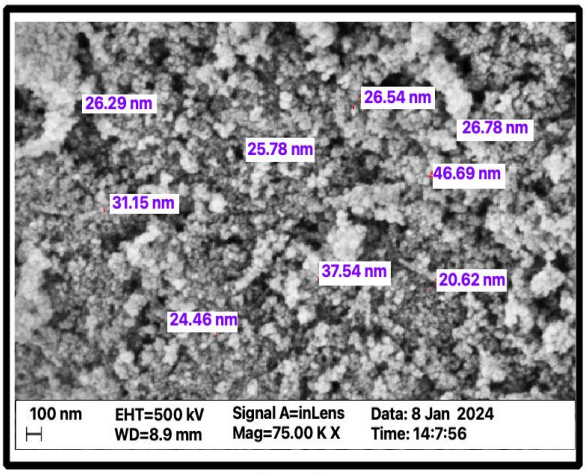

Figure 5. FE-SEM images of the 3D/GO/CNC@PAHA-AN dendrimer

At higher fields (beyond ±8000 Oe), the magnetization reaches saturation, with a saturation magnetization (Ms) of approximately 35 emu g^{-1}, indicating the high magnetic capacity of the synthesized dendrimer. When the applied field was removed (H = 0 Oe), a remanent magnetization of about 5 emu g^{-1} was observed, demonstrating the partial magnetic memory of the dendrimer after field removal.

The coercivity (Hc), representing the opposing magnetic field strength required to nullify the magnetization, was determined to be about 300 Oe. The low coercivity suggests that the dendrimer exhibits soft-magnetic behavior, meaning its magnetic polarity can be easily switched. These findings confirm that the 3D/GO/CNC@PAHA-AN nanocomposite exhibits soft-magnetic properties, making it a suitable candidate for magnetic separation and related applications [26].

3.2.3. *FE-SEM analysis of the magnetic nanocomposite 3D/GO/CNC@PAHA-AN*

The surface features, particle size, and morphology of 3D/GO/CNC@PAHA-AN were examined using FE-SEM, as illustrated in Fig. 5. Based on FE-SEM software analysis, particle sizes ranged from approximately 20.5 to 46.6 nm, with an average of 30–35 nm. These values are consistent with the expected dimensions for low- to mid-generation dendrimers (e.g., second- or third-generation). As illustrated in Fig. 5, the synthesized nanoscale, spherical dendrimers are uniformly distributed over the graphene oxide surface. This uniform dispersion facilitates rapid interaction with aflatoxin molecules. The dendrimers exhibited a porous structure, with spherical features clearly observed. This morphology increases the surface-to-volume ratio, thereby enhancing the adsorption kinetics of the magnetic nanocomposite [27]. In other words, the dendrimer surface contains pores and cavities that expand the accessible surface area and improve its adsorption efficiency. Ideal adsorbent materials exhibit these features and morphologies. The absence of significant aggregation and uniform particle distribution indicates successful grafting and dendritic growth on the underlying nanostructure [28, 29]. EDX analysis, a form of elemental spectroscopy, was used to determine the samples' elemental composition and chemical structure. The EDX results for the Raney Nickel-reduced and magnetically functionalized dendrimer showed three main elements: nitrogen (N), carbon (C), and oxygen (O), with weight percentages of 10.11%, 32.78%, and 57.11%, respectively. These elements correspond to the dendrimer's organic backbone and functional groups. The Ni peak indicates that a portion of the Raney Nickel catalyst remained in the sample. The high oxygen content suggests successful loading of magnetic metal oxide nanoparticles. The comparatively lower nitrogen content

10.57647/ijic.2026.1701.05

relative to carbon and oxygen indicates the presence of organic nitrogen-containing (amine) bonds within the dendrimer structure [30].

3.2.4. *TGA: Thermogravimetric Analysis*

Thermogravimetric analysis (TGA) was conducted to assess the thermal characteristics of GO and the 3D/GO/CNC@PAHA-AN dendrimer over the temperature range of 25–600 °C at a heating rate of 10 °C min^{-1}. The resulting thermograms are shown in Fig. 6. A comparison of the TGA profiles of pristine GO and dendrimer-modified GO indicates that grafting enhances thermal stability in the intermediate temperature range. The modified sample (GO-Dendrimer) shows a slower, more gradual weight loss due to organic branches and a lower density of oxidized groups, retaining a greater residue at higher temperatures (600 °C). The thermogram for 3D/GO/CNC@PAHA-AN shows an initial weight loss below 100 °C, attributed to the release of physically adsorbed water. The main thermal decomposition of the dendrimer backbone occurs between 200 and 500 °C. These findings suggest that incorporating dendrimers effectively enhances the thermal stability of the graphene structure in the composite [31].

3.2.5. *XRD analysis*

X-ray diffraction (XRD) is a non-destructive method for identifying the phase and crystal structure of materials and is suitable for both qualitative and quantitative analyses of crystalline substances. The XRD pattern of the synthesized magnetic nanocomposite was obtained to determine its crystal structure. The XRD pattern of 3D/GO/CNC@PAHA-AN is presented in Fig. 7.

3.3. Adsorption of aflatoxins B1, B2, G1, and G2 by

To evaluate the efficiency of the synthesized nanoadsorbent in extracting aflatoxins from contaminated solutions, recovery experiments were performed with standard aflatoxins.

The results of the intra-day recovery test (Table 1) show that the developed method using the nano-imprinted adsorbent extracted and quantified four aflatoxins (AFB1, AFB2, AFG1, and AFG2) at a spiking level of 10 ng g^{-1}, with high recoveries (94–95%) and low relative standard deviations (1.82–3.19%). These values indicate the method's high accuracy and precision and demonstrate its satisfactory performance and repeatability under intra-day conditions. Moreover, the close recovery values for all four aflatoxins confirm the adsorbent's uniform, nondiscriminatory performance, an essential advantage for analytical applications.

3.4. Adsorption isotherm models

To determine the adsorption isotherm, 10 mL solutions containing aflatoxin at standard concentrations of 5, 10, 20, 30, 40, and 60 µg L^{-1} were prepared. Subsequently, 1.5 mL of each solution was combined with 0.01 g of the synthesized nanoadsorbent and agitated at 400 rpm at room temperature for 1 hour. After agitation, the samples were centrifuged, and adsorption was evaluated by comparison with a standard solution. Additionally, 8.5 mL of the same aflatoxin solution without nanoadsorbent served as a blank. The experimental equilibrium data were analyzed using surface adsorption isotherm models to select the most appropriate model.

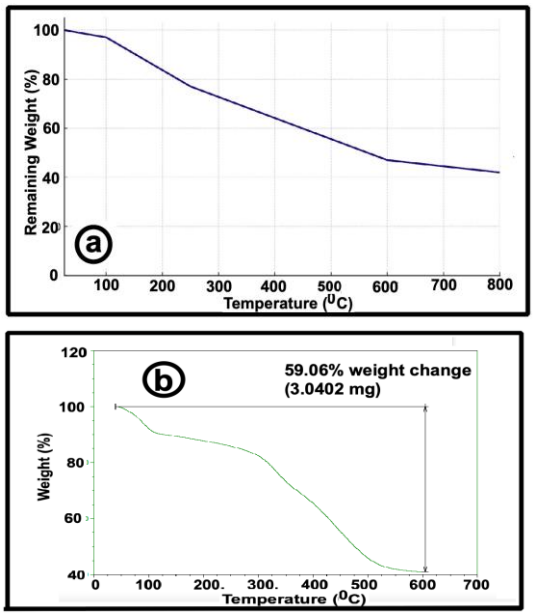

Figure 6. Thermograms of the samples: graphene oxide (GO) (a) and the 3D/GO/CNC@PAHA-AN dendrimer (b)

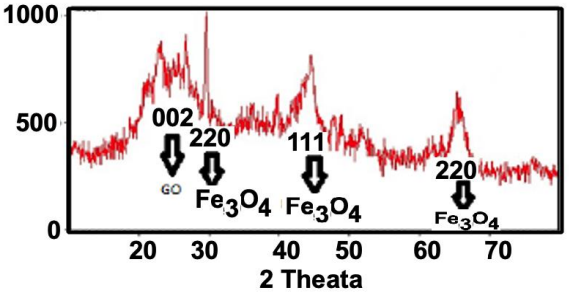

Figure 7. X-ray diffraction (XRD) pattern of the 3D/GO/CNC@PAHA-AN sample

Table 1. Recovery percentages of aflatoxins using 3D/GO/CNC@PAHA-AN nano adsorbent

	Spiking level	Recovery (%)	RSD (%)
AFB1	10 ng g^{-1}	94	3.19
AFB2	10 ng g^{-1}	95	2.79
AFG1	10 ng g^{-1}	94	2.13
AFG2	10 ng g^{-1}	95	1.85

10.57647/ijic.2026.1701.05

3.5. Adsorption isotherm

3.5.1. *Surface adsorption isotherm of aflatoxin B1 on 3D/GO/CNC@PAHA-AN nanoadsorbent*

The adsorption process between the adsorbent and adsorbate proceeds effectively until dynamic equilibrium is reached. In this study, equilibrium data for AFB_1 adsorption on 3D/GO/CNC@PAHA-AN were fitted to the Langmuir (Eq. 2), Freundlich (Eq. 3), Temkin (Eq. 4), Dubinin–Radushkevich (D-R, Eq. 5), and Redlich–Peterson (R-P, Eq. 6) isotherms. The determined isotherm parameters are presented in Table 2.

The Langmuir model assumes monolayer adsorption on a homogeneous surface and neglects interactions between adsorbed molecules. The dimensionless separation factor (RL) characterizes the adsorption process: $0 < R_L < 1$ indicates favorable adsorption, $R_L > 1$ indicates unfavorable adsorption, $R_L = 1$ indicates linear adsorption, and RL = 0 indicates irreversible adsorption. In this study, R_L ranged from 0.1028 to 0.5764, indicating that AFB_1 adsorption on the nanoadsorbent is favorable. The Freundlich model, in contrast, describes adsorption on a heterogeneous surface where the adsorption heat is distributed nonuniformly.

The parameter 1/n characterizes the adsorption type: if 1/n = 0, the process is irreversible; if $0 < 1/n < 1$, adsorption is favorable; and if $1/n > 1$, adsorption is unfavorable. The calculated 1/n value indicated favorable adsorption. The Temkin isotherm, with a positive B value, confirmed the exothermic nature of the adsorption reaction.

As indicated in Table 2, the R^2 value for the Langmuir model (0.9977) surpassed those of the Freundlich (0.9952), Temkin (0.9668), and D-R (0.928) models, suggesting that the Langmuir model provides the best fit. The Redlich–Peterson model combines Langmuir and the Freundlich approaches and is generally used over a wider concentration range. Based on the close R^2 values between Langmuir and the Freundlich isotherms, and the R-P modeling, the Langmuir isotherm appears to offer the best fit for describing aflatoxin adsorption. In this equation, q (mg g^{-1}) represents the maximum adsorption capacity, whereas K_L (L mg^{-1}) corresponds to the Langmuir equilibrium constant. The separation factor, R_L, is determined using: [33]

$$R_L = 1/1 + K_L\, Co \qquad (2)$$

$$\mathrm{Ln}\, q\, e = 1/n \ln C\, e + \ln K_F \qquad (3)$$

The parameter K_F (mg g^{-1} (L $mg^{-1})^{1/n}$) is the Freundlich isotherm constant. The parameter n represents the degree of surface heterogeneity, while K_F is strongly influenced by the adsorbent's adsorption capacity [34].

$$q_e = RT/b \ln C_e + RT/b \ln A \qquad (4)$$

In the Temkin isotherm model, A (L mg^{-1}) is the Temkin isotherm constant, and B is defined as RT/b. In this context, b (J mol^{-1}) represents the Temkin constant related to the heat of adsorption of aflatoxin, T (K) denotes the absolute temperature, and R is the universal gas constant. In this model, positive or negative values of B indicate exothermic or endothermic adsorption processes, respectively [35].

$$\mathrm{Ln}\, q_e = \ln q_s - k_{DR}\varepsilon 2 \qquad (4)$$

Where K_{DR} ($mol^2\ kJ^{-2}$) is the D-R constant related to surface energy absorption, and ε is the D-R isotherm constant [36].

$$\mathrm{Ln}\,(AC_e/q_e - 1) = g\,\mathrm{Ln}\,(C_e) + \mathrm{Ln}\,(B) \qquad (6)$$

In Eq. (7), B (mg L^{-1}) is the saturation constant of the isotherm, and g is a dimensionless constant [37].

3.6. Adsorption kinetics

3.6.1. *Kinetics of aflatoxin adsorption onto 3D/GO/CNC@PAHA-AN nanoadsorbent*

Adsorption kinetics examines the rate and mechanism of adsorbate transfer from the liquid or gas phase onto the adsorbent surface. Kinetic models help elucidate the adsorption of aflatoxins onto the adsorbent [38]. In this study, experimental data for the adsorption of aflatoxins onto 3D/GO/CNC@PAHA-AN were analyzed using three well-known kinetic models: pseudo-first-order (Lagergren) (Eq. 7), pseudo-second-order (Ho & McKay) (Eq. 8), and intra-particle diffusion (Weber & Morris) (Eq. 9). The determined kinetic parameters and associated R^2 values are summarized in Table 3. Comparison of results indicates that the pseudo-second-order model (R^2 = 0.9958) fits the experimental data better than the pseudo-first-order (R^2 = 0.9899) and intra-particle diffusion (R^2 = 0.9866) models. The intra-particle diffusion model alone does not adequately describe the adsorption of aflatoxins by 3D/GO/CNC@PAHA-AN, indicating that the rate-limiting step is not solely diffusion into the adsorbent's pores. The adsorption process appears to proceed through two or more stages. The first stage corresponds to rapid surface adsorption of aflatoxins onto the adsorbent. In contrast, the second stage involves gradual diffusion of aflatoxins into the adsorption sites, where intra-particle diffusion is rate-controlling.

$$\mathrm{Log}\,(q_e - q_t) = \log q_e - K_1 t/2{,}303 \qquad (7)$$

$$t/qt = 1/K^2 qe^2 + t/q_e \qquad (8)$$

$$q_t = k_p\, t^{1/2} + C_i \qquad (9)$$

Here, q_t (mg g^{-1}) denotes the adsorption capacity at time t. In contrast, k_1 (min^{-1}), k_2 (g mg^{-1} min^{-1}), and k_i (mg g^{-1} min^{-1}) denote the rate constants for the pseudo-first-order, pseudo-second-order, and intra-particle diffusion models, respectively. C_i denotes the boundary layer thickness [39-41].

10.57647/ijic.2026.1701.05

Table 2. Adsorption isotherm model parameters for AFB1 on the 3D/GO/CNC@PAHA-AN nano-adsorbe

Adsorption Isotherm	Parameters	AFLB1	R^2
Langmuir	q_{max} (mg/g)	16.85	0.9977
	K_L (L/mg)	0.15	
	R_L	0.5764 – 0.1028	
Freundlich	K_f (mg/g)(L/mg)$_{1/n}$	0.00854	0.9952
	1/n	0.8291	
Temkin	A (L/mg)	0.2455	0.9668
	B (J/mol)	1.1364	
Dubinin–Radushkevich	q_s (mg/g)	1.808	0.928
	K_{DR} (mol^2 / kJ^2)	1×10^{-5}	
Redlich–Peterson	A (dm^3/g)	13.39	0.9922
	B (dm^3/mg)	0.0747	
	G	0.9232	

Table 3. Kinetic model parameters for the surface adsorption of aflatoxins onto 3D/GO/CNC@PAHA-AN nano adsorbent

Kinetic	Parameters	AFLB1	R^2
Pseudo-First-Order Kinetic Model	K_1 (min^{-1})	0.1673	0.9899
	q_e (mg g^{-1})	1.014	
Pseudo-Second-Order Kinetic Model	K_2 (g mg^{-1}) min^{-1}	1.375	0.9958
	q_e (mg g^{-1})	0.9735	
Intra-particle diffusion-Weber & Morris	K_i (g mg^{-1}) min$^{-1/2}$	0.3702	0.9866
	C_i (mg g^{-1})	1.1865	

4. Conclusion

The 3D/GO/CNC@PAHA-AN nanoadsorbent demonstrated high efficiency as a magnetic adsorbent for separating aflatoxins, particularly AFB1, from contaminated samples. HPLC has been shown to be an accurate, swift, and user-friendly technique for the detection and quantification of aflatoxins, providing a viable alternative to less reliable methods. The high recovery rates indicate the potential of this nanoadsorbent as a supporting tool in chromatographic methods, enhancing accuracy and reliability in aflatoxin analysis. Key advantages of the synthesized nanoadsorbent include high adsorption efficiency, preservation of aflatoxin structural integrity during adsorption, stable signal responses, and selective affinity for target compounds. Moreover, the method's minimal reliance on organic solvents underscores its environmental friendliness, making it suitable for both analytical and eco-conscious applications.

Notes

This work is part of the first author's graduate thesis research.

Authors Contribution

All the authors have participated sufficiently in the intellectual content, conception and design of this work or the analysis and interpretation of the data (when applicable), as well as the writing of the manuscript.

Availability of data and materials

The data that support the findings of this study are available from the corresponding author, upon reasonable request.

Conflict of interests

The author states that there is no conflict of interest.

References

[1] R. Karami-Osboo, M. Mirabolfathy, R. Kamran, M. Shetab-Boushehri, S. Sarkari, Aflatoxin B1 in maize harvested over 3 years in Iran, Food Control, 23 (2012) 271-274.

[2] R. Karami-Osboo, M. Mirabolfathi, A novel dispersive nanomagnetic particle solid-phase extraction method to determine aflatoxins in nut and cereal samples, Food Analytical Methods, 10 (2017) 4086-4093.

[3] S. Marin, A. Ramos, G. Cano-Sancho, V. Sanchis, Mycotoxins: Occurrence, toxicology, and exposure assessment, Food and chemical toxicology, 60 (2013) 218-237.

[4] M. Mirabolfathy, R.K. Osboo, V. Rahjoo, Important mycotoxins, Iran status, Annu. Rev. Res, 5 (2019) 1-10.

[5] Y.Y. Gong, S. Watson, M.N. Routledge, Aflatoxin exposure and associated human health effects, a review of epidemiological studies, Food safety, 4 (2016) 14-27.

[6] G. Miklós, C. Angeli, Á. Ambrus, A. Nagy, V. Kardos, A. Zentai, K. Kerekes, Z. Farkas, Á. Jóźwiak, T. Bartók, Detection of aflatoxins in different matrices and food-chain positions, Frontiers in Microbiology, 11 (2020) 1916.

[7] F. Wu, Global impacts of aflatoxin in maize: trade and human health, World Mycotoxin Journal, 8 (2015) 137-142.

[8] Tavassoty Kheiry B.,Tadayon F., Ahmad Panahi H., Moniri E., Design of Temperature-Sensitive Hydrogel Nanoparticles and Investigation of Their Application in the Development of a New Generation of Anti-Cancer Drugs with Optimization Conditions by Central Composite Design. Int. J. Ind. Chem.,2025; 16(2). 1-14.
http://doi.org/10.57647/j.ijic.2025.1602.12

[9] J.H. Williams, T.D. Phillips, P.E. Jolly, J.K. Stiles, C.M. Jolly, D. Aggarwal, Human aflatoxicosis in developing countries: a review of toxicology, exposure, potential health consequences, and interventions, The American journal of clinical nutrition, 80 (2004) 1106-1122.

[10] H. Contraception, H. Therapy, IARC monographs on the evaluation of carcinogenic risks to humans, Lyon: International Agency for Research on Cancer, (1999).

[11] Torabi Fard N, Tadayon F, Ahmad Panahi H, Moniri E. Synthesis,characterization and application of a novel three-dimensional magnetic graphene oxide decorated with polyester dendrimers for detection of donepezil hydrochloride in pharmaceutical formulation and biological fluid. Journal of Molecular Liquids. 2022; 365:118149.
http://doi.org/10.1016/j.molliq.2021.118149

[12] M. Selin, S. Nummelin, J. Deleu, J. Ropponen, T. Viitala, M. Lahtinen, J. Koivisto, J. Hirvonen, L. Peltonen, M.A. Kostiainen, High-generation amphiphilic Janus-dendrimers as stabilizing agents for drug suspensions, Biomacromolecules, 19 (2018) 3983-3993.

[13] M. Liu, K. Kono, J.M. Fréchet, Water-soluble dendritic unimolecular micelles:: Their potential as drug delivery agents, Journal of Controlled Release, 65 (2000) 121-131.

[14] M. Inagaki, F. Kang, M. Toyoda, H. Konno, Graphene: Synthesis and preparation, Advanced materials science and engineering of carbon, (2014) 41-65.

[15] J. Liu, L. Cui, D. Losic, Graphene and graphene oxide as new nanocarriers for drug delivery applications, Acta biomaterialia, 9 (2013) 9243-9257.

[16] M.Y. Alazaiza, A. Albahnasawi, G.A. Ali, M.J. Bashir, N.K. Copty, S.S.A. Amr, M.F. Abushammala, T. Al Maskari, Recent advances of nanoremediation technologies for soil and groundwater remediation: A review, Water, 13 (2021) 2186.

[17] L. Giraldo, A. Erto, J.C. Moreno-Piraján, Magnetite nanoparticles for removal of heavy metals from aqueous solutions: synthesis and characterization, Adsorption, 19 (2013) 465-474.

[18] F. Yang, J. Li, T. Chen, W. Ren, C. Gao, J. Lin, C. Xu, X. Ma, J. Xing, H. Bao, Applications of magnetic nanoparticles for boundarics in biomedicine, Fundamental Research, (2025).

[19] R. Karami-Osboo, L. Faramarz, Rapid Aflatoxin Detection in Black Tea Using Fe3O4 Magnetic Nanoparticle, Food Analytical Methods, 17 (2024) 1189-1194.

[20] X. Liu, Z. Ma, J. Xing, H. Liu, Preparation and characterization of amino–silane modified superparamagnetic silica nanospheres, Journal of Magnetism and magnetic Materials, 270 (2004) 1-6.

[21] Y. Liu, S. Huang, X. Zhao, Y. Zhang, Fabrication of three-dimensional porous β-cyclodextrin/chitosan functionalized graphene oxide hydrogel for methylene blue removal from aqueous solution, Colloids and Surfaces A: Physicochemical and Engineering Aspects, 539 (2018) 1-10.

[22] D.R. Dreyer, S. Park, C.W. Bielawski, R.S. Ruoff, The chemistry of graphene oxide, Chemical society reviews, 39 (2010) 228-240.

[23] S. Stankovich, D.A. Dikin, G.H. Dommett, K.M. Kohlhaas, E.J. Zimney, E.A. Stach, R.D. Piner, S.T. Nguyen, R.S. Ruoff, Graphene-based composite materials, nature, 442 (2006) 282-286.

[24] A. Sardinha, FTIR Spectra of Graphene Oxide, Instituto Nacional de Pesquisas Espaciais: São José dos Campos, São Paulo, Brazil, (2019).

[25] C.C. Berry, A.S. Curtis, Functionalisation of magnetic nanoparticles for applications in biomedicine, Journal of physics D: Applied physics, 36 (2003) R198.

[26] D. Gao, D.-D. Wang, Q.-F. Fu, L.-J. Wang, K.-L. Zhang, F.-Q. Yang, Z.-N. Xia, Preparation and evaluation of magnetic molecularly imprinted polymers for the specific enrichment of phloridzin, Talanta, 178 (2018) 299-307.

[27] O. Semong, Development of an aflatoxin B1 specific molecularly imprinted solid phase extraction sorbent for the selective pre-concentration of toxic aflatoxin B1 from child weaning food, Tsabana, in, Botswana International University of Science and Technology (Botswana), 2016.

[28] Z.S.G. Hashemipour, F. Tadayon, O.R. KARAMI, Preparation of Magnetic Nano Composite Modified with Orange Peel for Adsorption of Vitamin B5 from Aqueous Solution, (2022).

[29] J.I. Goldstein, D.E. Newbury, J.R. Michael, N.W. Ritchie, J.H.J. Scott, D.C. Joy, Scanning electron microscopy and X-ray microanalysis, springer, 2017.

[30] T. Hatakeyama, F.i. Quinn, Thermal analysis: fundamentals and applications to polymer science, [sl], 1999.

[31] N. Nakagiri, M. Manghnani, L. Ming, S. Kimura, Crystal structure of magnetite under pressure, Physics and Chemistry of Minerals, 13 (1986) 238-244.

[32] T.W. Weber, R.K. Chakravorti, Pore and solid diffusion models for fixed-bed adsorbers, AIChE Journal, 20 (1974) 228-238.

[33] H. Freundlich, Über die adsorption in lösungen, Zeitschrift für physikalische Chemie, 57 (1907) 385-470.

[34] A. Boisen, S. Dahl, J.K. Nørskov, C.H. Christensen, Why the optimal ammonia synthesis catalyst is not the optimal ammonia decomposition catalyst, Journal of Catalysis, 230 (2005) 309-312.

[35] J. Rouquerol, F. Rouquerol, P. Llewellyn, G. Maurin, K. Sing, Adsorption by powders and porous solids: principles, methodology and applications, Academic press, 2013.

[36] F.-C. Wu, B.-L. Liu, K.-T. Wu, R.-L. Tseng, A new linear form analysis of Redlich–Peterson isotherm equation for the adsorptions of dyes, Chemical Engineering Journal, 162 (2010) 21-27.

[37] K.Y. Foo, B.H. Hameed, Insights into the modeling of adsorption isotherm systems, Chemical engineering journal, 156 (2010) 2-10.

[38] A.B. Albadarin, M. Charara, B.J.A. Tarboush, M. Ahmad, T.A. Kurniawan, M. Naushad, G.M. Walker, C. Mangwandi,

Mechanism analysis of tartrazine biosorption onto masau stones; a low cost by-product from semi-arid regions, Journal of Molecular Liquids, 242 (2017) 478-483.

[39] S. Suganya, P.S. Kumar, Kinetic and thermodynamic analysis for the redemption of effluents containing Solochrome Black T onto powdered activated carbon: a validation of new solid-liquid phase equilibrium model, Journal of Molecular Liquids, 259 (2018) 88-101.

[40] Z. Berizi, S.Y. Hashemi, M. Hadi, A. Azari, A.H. Mahvi, The study of non-linear kinetics and adsorption isotherm models for Acid Red 18 from aqueous solutions by magnetite nanoparticles and magnetite nanoparticles modified by sodium alginate, Water Science and Technology, 74 (2016) 1235-1242.

10.57647/ijic.2026.1701.05